MAGNETOHYDRODYNAMICS Vol. 50 (2014), No. 1, pp. 19–26

BREAKUPS OF MAGNETIC CHAINS IN AN OSCILLATING FIELD

Yan-Hom Li[1], *Ekansh Bansal*[1,2], *Ching-Yao Chen*[2*]

[1] *Department of Mechanical Engineering, National Chiao Tung University, Taiwan, ROC*

[2] *Department of Mechanical Engineering, Indian Institute of Technology Bombay, India*

[*] *Corresponding author, e-Mail: chingyao@mail.nctu.edu.tw*

This article outlines and illustrates the manipulations and rupture mechanisms of micro magnetic chains by experimental and numerical analysis. A reversible micro-chain consisting of micro-meter superparamagnetic particles is formed under a static directional field and manipulated by an additional dynamical perpendicular field. We demonstrate the chains' different behaviors from rigid body oscillations and bending distortions to rupture failures. By calculating the induced drag and the normal force, which dominate the deformation and ruptures of the chains, we find that the distortions and ruptures occur at the position between the two particles, which sustain significant drag variation with respect to the normal force.

1. Introduction. Magnetorheological (MR) suspension is an artificial and smart fluid consisting of paramagnetic solid particles suspended in a nonmagnetic solvent. Due to the paramagnetism of these particles, they are useful to produce reversible micro devices such as pumps, actuators, mixers [1–3] and artificial swimmers [4–6], which can be utilized in micro channels and further applied in advanced biotechnical devices or micro-electro-mechanical-systems (MEMS).

The dynamics of MR suspensions under a rotating magnetic field has been studied extensively in recent years [7–9]. It has been shown that the flexible magnetic chain in a rotating field would be bent and rotating synchronously with the field under the critical frequency [10]. When an excessive frequency occurs, the dynamics becomes asynchronous with back-and-forth rotations [11]. The dependence of the cross-over frequency on the viscosity of the carrier fluid was analyzed by applying a rotating field of constant amplitude to suspensions. In addition, researches have also revealed numerical results regarding various breakages of the chains under a rotating field by varying the Mason number, a dimensionless parameter expressing the ratio of viscous forces to the dipolar forces [9, 12].

To effectively apply the micro-chains in MEMS, detailed studies regarding manipulations of the chains are strongly desired. The deformation of magnetic chains under an oscillating field has been studied by investigating the elastic properties of magnetic chains or filaments linked by DNA [13,14]. Thorough experiments have been conducted and illustrate that the chains would evolve from rigid body motion deformation to breakup due to the induced drag under a higher oscillating field [5,15,16,17]. Based on the experimental results, a criterion is proposed to determine the structural stability [15]. Similar asynchronous behaviors of the chain to the external field as reported in a rotating field [11], a phenomenon referred to as "trajectory shift", is identified if the instantaneous phase lag is greater than $\pi/2$ [16,17]. This asynchronous behavior is successfully applied to steer the swimming orientations of a micro-swimmer consisting of magnetic beads [6, 16].

In this paper, we first review different types of oscillations of a micro-chain driven by an oscillating field, such as rigid body motion deformation to rupture

mentioned above. Since the main factor causing the chain's deformation or rupture is the local ratio between drag to normal force, our main task is to numerically calculate the drag acting on each particle of the chain and realize the relationship of the distribution of drag between particles to the rupturing mechanism.

2. Experimental setup. The magnetorheological suspensions used in our experiment are water suspensions of polystyrene (PS) microspheres coated with iron oxide grains. The aqueous suspensions (Dynabeads M-450 Epoxy by Invitrogen Life Technologies), whose mean diameters are $4.5\,\mu$m with a susceptibility of $\chi = 1.6$, exhibit superparamagnetic behavior with no hysteresis or magnetic remanence. This property can be utilized to make reversible magnetic chains. A unidirectional magnetic field generated by a pair of coils connected to a DC power source is used to aggregate the particles and form chains. To create an oscillating field, we set another perpendicular pair of coils connected to an AC power supply, which generates sinusoidal electric signals. Based on the field configuration, the overall oscillating field $\mathbf{H} = H_\mathrm{d}\mathbf{i} + H_\mathrm{v}\mathbf{j}$, in which $\mathbf{i}$ and $\mathbf{j}$ are the unit vectors in the directional and perpendicular axis, respectively, is composed by a dynamical perpendicular field H_v with a maximum field strength H_p and frequency f, i.e. $H_\mathrm{v} = H_\mathrm{p}\sin(2\pi ft)$, and a static directional field H_d. The effects of the field strength on the behaviors of particle chains can be realized by varying the strength of the oscillating field and observing the structural stabilities of the chains. More detailed layouts of the experimental setup are given in [15,16,17]. All the motions of the chains are observed and recorded by an optical microscope. Multiple experiments, in which the chains experience structural breakups, are carefully documented for relevant conditions of ruptures, such as the timings and locations of ruptures. The force distribution acting on the particles at the timings of breakups is simulated to study its relationship to the occurrences of breakups.

3. Results and discussion.

3.1. Reviews of oscillating modes. By increasing the strength of the oscillating field or the chain length, the chains demonstrate different behaviors from rigid body oscillations, bending deformation to breakup failures [5, 15]. Additionally, the chains oscillate almost synchronously with the magnetic field but lagging behind by a periodically changeable phase angle, which is caused by the induced hydrodynamic drag. Detailed analysis regarding the motion of an oscillating chain is reported in [5, 15, 16, 17]. For readers' convenient references, typical cases are demonstrated below to identify their characteristic behaviors.

Fig. 1 shows the sequential images of a chain of 10 particles (denoted as a P10 chain) formed by a directional magnetic field of $H_\mathrm{d} = 24.15\,$Oe and oscillating with the perpendicular field strength of $H_\mathrm{p} = 29.02\,$Oe within one period. The chain oscillates as a rigid body and nearly synchronously with the magnetic field but lagging behind by a slight changeable phase angle $\triangle\theta_\mathrm{L}$.

Hence, the motion of the superparamagnetic chain is dominated by the magnetic torque and induced hydrodynamic drag, or the dimensionless Manson number. To demonstrate the chain's deformation, a longer P15 chain under a stronger oscillating field of $H_\mathrm{p} = 48.02\,$Oe and a weaker directional field strength of $H_\mathrm{d} = 17\,$Oe is depicted in Fig. 2. The significant bending deformation is resulted associated with larger instantaneous lagging angles than the P10 chain shown in Fig. 1. Nevertheless, no structural ruptures are observed.

In order to record the rupture behaviors of the particle chains, the amplitude of the oscillating field is increased until the breaking failure. Fig. 3 shows the sequential images of an oscillating P15 chain evolving from bending distortion to breaking failures on two sides. At the time $t = 18/30\,$P, the chain breaks into

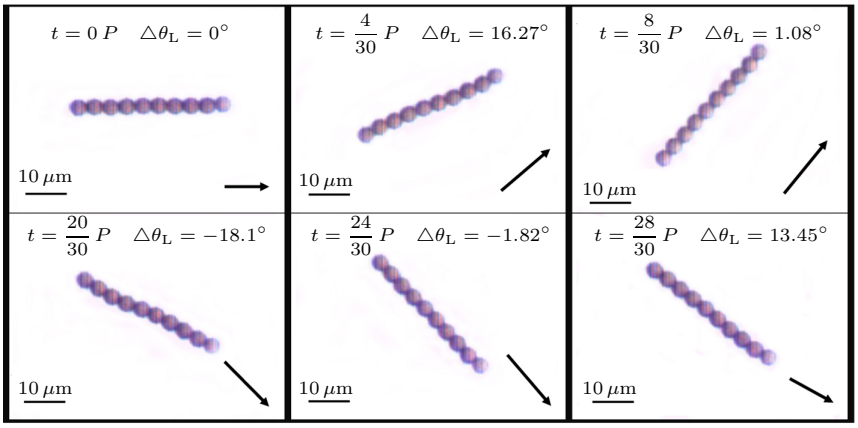

Fig. 1. Sequential images of a chain consisting of 10 particles (denoted as P10 chain) oscillating nearly as a rigid body. The chain is subjected to a frequency of $f = 1\,\mathrm{Hz}$. The black arrow indicates the direction and magnitude of the overall magnetic field, with P being the oscillating period of the field.

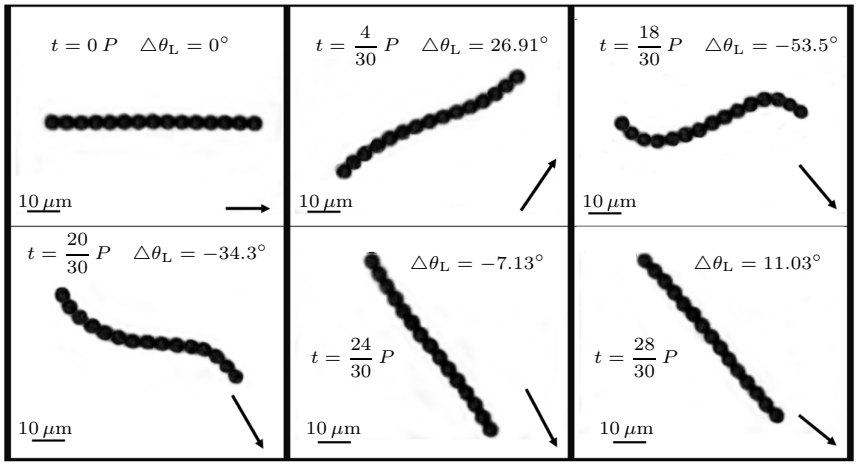

Fig. 2. Sequential images of a P15 chain under a stronger oscillating field (video online: http://www.youtube.com/watch?v=qwTDnKPbQJs). Bending deformation is apparently observed. The most severe distortion shown as S-shape occurs at the time $t = (18/30)\,P$, in which the chain experiences the largest lagging angle of $|\triangle\theta_{\mathrm{L}}| = 53.5°$.

three smaller segments to oscillate individually, with the field but lagging behind by slightly different phase angles, which depend on the length of the chain.

3.2. Dynamics analysis and simulations. To analyze the detailed motion of an oscillating chain, four stages of the chain's motion can be classified within half period of oscillation, i.e. $0 < t < P/2$, as demonstrated in Fig. 4. Note that due to the phase lag, the time indicated here is measured based on the oscillating chain, not the external field. By observing the rupture process of the chain, we learn that the breakups of the chains often occur in a duration of $P/4 < t < P/2$ (stage 4), as a typical example shown in Fig. 3. The reason results of such a rupture can be understood by inspecting the magnitude of the dipolar forces acting on the chain and instantaneous angular speed at each stage.

It is understandable that the normal dipolar attraction between the beads sustain the chaining stability, while the induced drag acting azimuthally to the

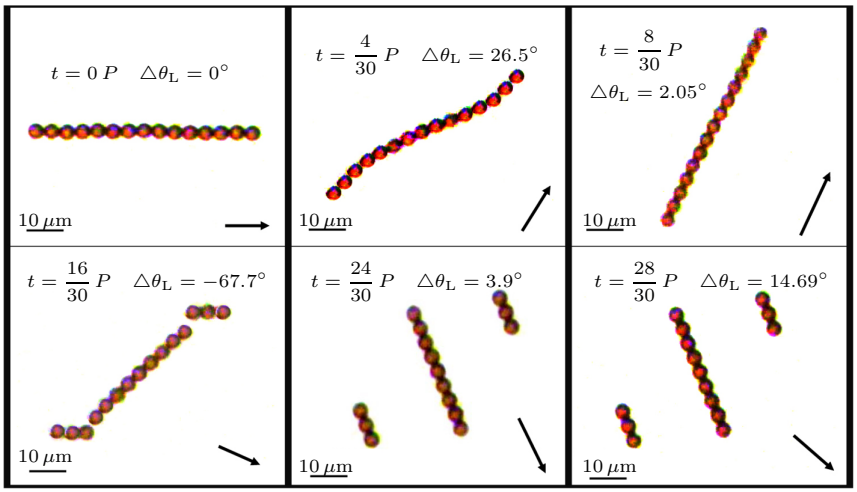

Fig. 3. Sequential images of a P15 chain evolving from bending distortion to breaking failures on two sides (video online: http://www.youtube.com/watch?v=dKBJK9aooBE). The strength of the perpendicular is increased to $H_{\mathrm{p}} = 56.72$ Oe.

chain would lead to structural rupture. By the Stokes theorem, the induced drag of a single sphere is proportional to its speed. As a result, it can be easily concluded that the chain is most likely to rupture at the stage of higher angular speed and weaker overall field strength. By inspecting the field of $\mathbf{H} = H_{\mathrm{d}}\mathbf{i} + \mathbf{H}_{\mathrm{v}}\mathbf{j}$ with a constant H_{d} and a time-dependent $H_{\mathrm{v}} = H_{\mathrm{p}}\sin(2\pi ft)$, the chain is more stable within stage 2 ($0 < t < P/4$), when it decelerates toward the stagnation point (stage 3 at $t = P/4$) associated with an increasing field strength. On the contrary, the chain starts to accelerate with a weakening overall field strength within stage 4 ($P/4 < t < P/2$) and thus it is the most unstable stage. The argument is in line with the findings in experiments.

As discussed above, while the chain steps into the fourth stage (oscillating clockwise), the chain experiences an accelerated process, in which the hydrodynamics drag increases. In the meantime, the normal magnetic forces decline and lead to this time interval more unstable. It is known that when the hydrodynamics drag acts on the chain azimuthally, each particle obtains an angular acceleration adverse to its oscillating direction (counter-clockwise), as depicted in Fig. 5. When

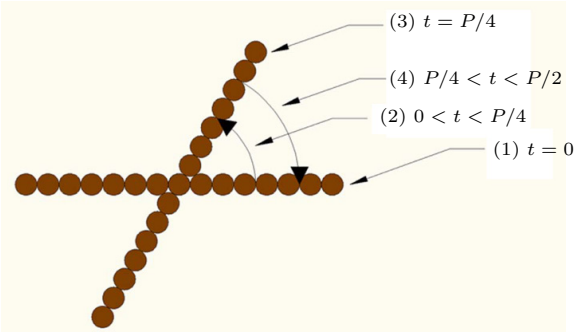

Fig. 4. Scheme of 4 stages within the first half period of oscillation. The chain accelerates associated with a weakening overall field strength within stage 4 ($P/4 < t < P/2$), when it is the most unstable time interval to rupture the chain.

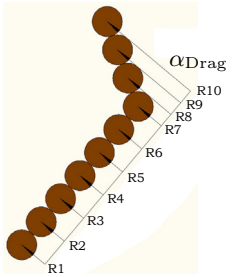

Fig. 5. Schematic representation of the adverse angular acceleration induced by local drags to variant particles in a representative P20 chain. Only half part of the chain is sketched, such that the letter "R" denotes the right half of the chain. The numbers at "R" show the serial number of beads.

the adverse accelerations of the two adjacent particles are discrepant, one particle of the two slips from the other, which results in the deformation of the chain. Once the bounding force between the particles cannot sustain the drag force, the breakup of the chain occurs.

In order to investigate the forces acting on the oscillating chains, dynamics simulations are performed by the commercial software FLUENT. Moving meshes that exactly match the motions of oscillating chains in the experiments are first prescribed. Transient simulations lasting for a period of oscillation are then carried out based on the prescribed moving grid. The results at the timings of breakups for the correspondent cases are taken for further analysis. Fig. 6 shows a typical grid structure of the 3D meshes at $t = 0\,P$. Multiple simulations under the identical physical conditions of the experiments are conducted to calculate the induced drags of chains consisting of various numbers of particles.

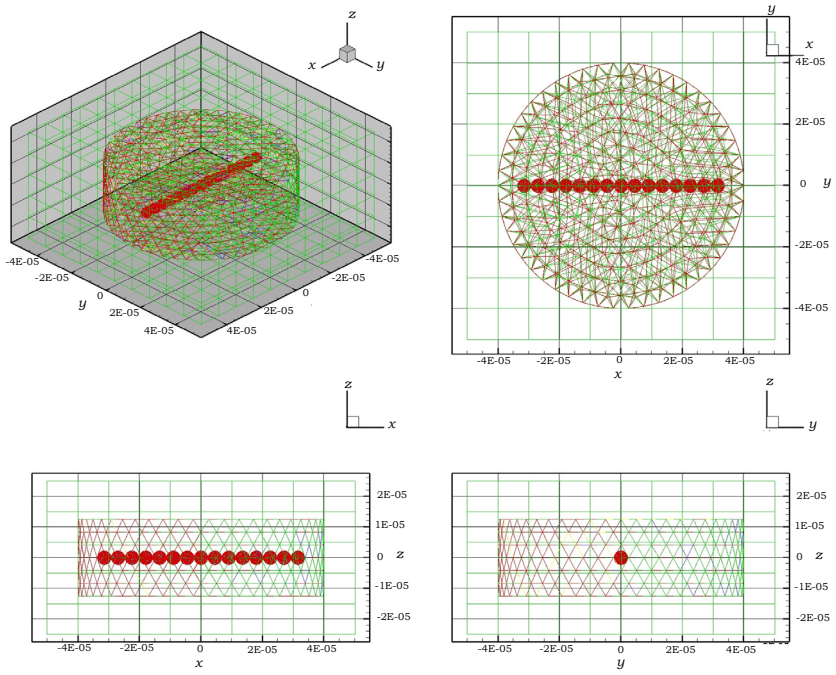

Fig. 6. Sketches of a typical grid structure of 3D meshes at $t = 0\,P$ for simulating the drag acting on a P15 chain.

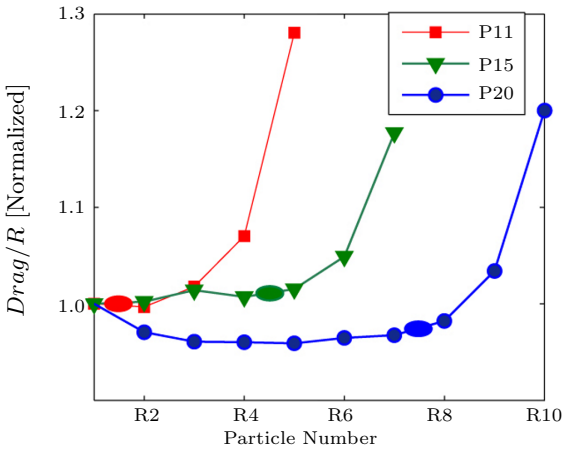

Fig. 7. Comparison of normalized drag on three chains of different lengths at their corresponding rupture timings. Only the particles in the right-half part of the chain are shown. The oval-shaped marks indicate the rupture position of chains observed in experiments. Chain rupture always occurs at the position, where the normalized drag shows a significant increase.

Based on the experimental results and reasons stated in the previous section, ruptures of oscillating chains would most likely occur within stage 4. Findings from the transient simulations of the oscillating chains reveal that the total drag acting on a certain particle increases monotonically to its corresponding radial length (denoted as R), which represents the distance from the center of the chain to the center of this particular particle. The normalized drags, i.e. $Drag/R$, to all the individual particles at the timings of rupture are shown in Fig. 7. The locations of breakups of their correspondent experiments are also marked in the figure. The results indicate a nearly constant value for the inner particles, which remain structurally stable. Nevertheless, the ruptures always occur at the positions, where the normalized drags appear significantly increased. The results are consistent with the arguments stated in Fig. 5, such that the location of rupture would occur if the induced drags between two adjacent particles exhibit significant variations.

In addition, the rupture of a chain can also be analyzed by the competition between the induced drag force, which acts in the direction perpendicular to the oscillating axis (or azimuthally to the chain) depicted in Fig. 5, and the normal magnetic force pointed along the oscillating axis. It is noteworthy to restate that while the drag force is the main factor to cause rupture, the actual force sustaining the chaining structure is the tangential friction induced by the normal magnetic force. Even the magnitude of friction is not available, it can be represented by the normal force because of the proportionality between them. The drag force is found through simulations. On the other hand, the magnetic normal force due to the dipolar attraction between the N^{th} and $(N+1)^{\text{th}}$ sub-particles can be calculated by equations as shown [17]:

$$F(N) = F(N-1) + F_D^N, \quad \text{for } N > 1, \tag{1}$$

$$[F(1), F(n)] = [F_D^1, F_D^n], \quad \text{for } N = 1. \tag{2}$$

In the above equations, F_D^i is the magnetic dipolar interaction between an i^{th}

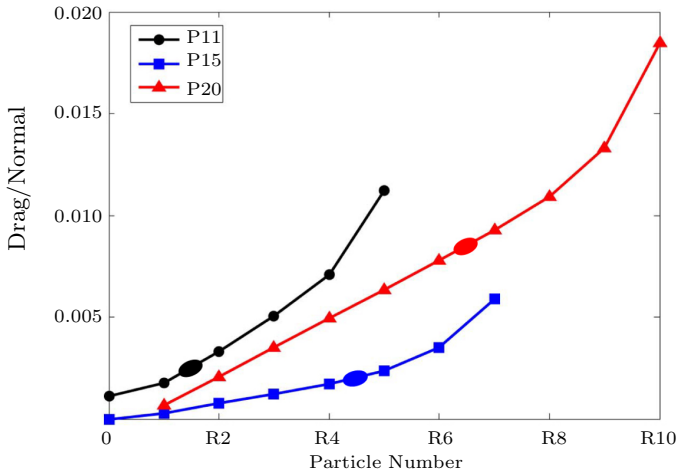

Fig. 8. Ratios between the induced viscous drags to normal dipolar forces acting on individual particles. The oval-shaped marks indicate the rupture position of chains. The variations evolve from nearly linear to cubic near the position of breakups.

particle and the rest of the particles in the chain and is given by

$$F_D^i = \frac{3\mu_0 m^2}{4\pi}\left(1 - 3\cos^2\alpha\right)\left[\sum_{j=-N}^{i-1}\frac{1}{r_{ij}^4} - \sum_{j=i+1}^{N}\frac{1}{r_{ij}^4}\right]. \tag{3}$$

Here, $r_{ij} = |r_i - r_j| = 2a|i-j|$ is the distance between the centers of the i^{th} and j^{th} particles, and α is the angle between the long axis of the chain and the overall magnetic field. μ_0 and m represent the vacuum permeability and the dipole moment, respectively. Here we do not consider the centrifugal force because it is confirmed to be negligible with respect to the dipole interaction force. The ratio between the drag force and the normal force is demonstrated in Fig. 8, and evolves from a nearly linear to cubic variation near the position of breakup, which indicates the dominance of the drag force over the frictional force and further affirms the agreements of simulations with the experimental observations.

4. Concluding remarks. The present article reviews three types of oscillating modes observed in the experiments, i.e. rigid body oscillation, bending deformation and rupture instability, when a micro-chain consisting of magnetic beads is subjected to an oscillating field. To realize the rupturing mechanism, numerical simulations were carried out to obtain the induced viscous drag acting on individual particles. Consequently, competitions between the induced drag and normal dipolar forces between the particles were analyzed. It is found that the rupture occurs at the position between the two particles, which sustain significant drag variation with respect to the radial length and normal force.

Acknowledgements. The authors are in debt to the reviewer for providing important references to our attention. The financial support by the National Science Council of Taiwan (R.O.C.) through Grant NSC 99-2221-E-009-057-MY3 is acknowledged.

REFERENCES

[1] S.L. Biswal, and A.P. Gast. *Anal. Chem.*, vol. 76 (2004), issue 21, pp. 6448–6455.

[2] R. Tamal, S. Ashok, C. Sayan, G. Ranjan, K.P. Ishwar. *Phys. Fluids*, vol. 21 (2009), p. 027101.

[3] J.E. Martin, L. Shea-Rohwer, K.J. Solis. *Phys. Rev. E*, vol. 80 (2009), p. 016312.

[4] R. Dreyfus, J. Baudry, M.L. Roper, M. Fermigier, H.A. Stone. *J. Bibette. Nat.*, vol. 437 (2005), p. 862.

[5] Y.-H. Li, S.-T. Sheu, J.M. Pai, C.-Y. Chen. *J. Appl. Phys.*, vol. 111 (2012), p. 07A924.

[6] Y.-H. Li, H.-C. Lin, C.-Y. Chen. *IEEE Trans. Magn.*, 49 (2013), no. 7, pp. 4120–4123.

[7] S. Melle, J.E. Martin. *J. Chem. Phys.*, vol. 118 (2003), p. 21.

[8] A. Vuppu, A. Garcia, M. Hayes. *Langmuir*, vol. 19 (2003), p. 8646.

[9] I. Petousis, E. Homburg, R. Derks, A. Dietzel. *Lab Chip* , vol. 7 (2007), p. 1746.

[10] A. Cebers, I. Javaitis. *Phys. Rev. E*, vol. 69 (2004), p. 021404.

[11] B. Frka-Petesic, K. Erglis, J.F. Berret, A. Cebers, V. Dupuis, J. Fresnais, O. Sandre, R. Perzynski. *JMMM*, vol. 323 (2011), p. 1309.

[12] T.G. Kang, M.A. Hulsen, P.D. Anderson, J.M.J. den Toonder, H.E.H. Meijer. *Phys. Rev. E*, vol. 76 (2007), p. 066303.

[13] K. Erglis, D. Zhulenkovs, A. Sharipo, A. Cebers. *J. Phys.: Condens. Matter*, vol. 20 (2008), p. 204107.

[14] K. Ērglis, V. Ose, A. Zeltins, A. Cēbers. *Magnetohydrodynamics*, vol. 46 (2010), no. 1, pp. 23–29.

[15] Y.-H. Li, C.-Y. Chen, S.-T. Sheu, J.-M. Pai. *Microfluid Nanofluid*, vol. 13 (2012), no. 4, pp. 1579–588.

[16] Y.-H. Li, H.-C. Lin, C.-Y. Chen. . *Microfluid Nanofluid*, 14 (2013), no. 5, pp. 831–838.

[17] H.-C. Lin, Y.-H. Li, C.-Y. Chen. . *Microfluid Nanofluid*, published online (DOI: 10.1007/s10404-013-1286-6).

Received 01.04.2013